Prediction of Unsteady Blade Surface Pressures on an Advanced Propeller at an Angle of Attack

M. Nallasamy*
Sverdrup Technology, Inc., Brook Park, Ohio 44142
and
J. F. Groeneweg†
NASA Lewis Research Center, Cleveland, Ohio 44135

This paper considers the numerical solution of the unsteady three-dimensional Euler equations to obtain the blade surface pressures of an advanced propeller at an angle of attack. The specific configuration considered is the SR7L propeller at cruise conditions with a 4.6-deg inflow angle corresponding to the + 2-deg nacelle tilt of the propeller test assessment flight test condition. The results indicate nearly sinusoidal response of the blade loading, with angle of attack. For the first time, detailed variations of the chordwise loading as a function of azimuthal angle are presented. It is observed that the blade is lightly loaded for part of the revolution and shocks appear from hub to about 80% radial station for the highly loaded portion of the revolution.

Introduction

ADVANCED propeller tests in wind tunnels and in flight have been conducted to understand the aerodynamics and acoustics of advanced designs. Aerodynamic tests of the 9-ft-diam, single rotation SR7L NASA/Hamilton standard design were run in a transonic wind tunnel in Modane, France. Blade surface steady and unsteady pressures were measured during early 1987 on a two-blade configuration.[1-3] (The complete eight-blade propeller was not tested due to drive power limitations.) The propfan test assessment (PTA) flight program (1987–1988) was managed by Lockheed Aeronautical Systems Company under a contract to the NASA Lewis Research Center. The 9-ft propfan was flight tested on a modified, instrumented Gulfstream GII business jet (Fig. 1). The objectives of the PTA program were to evaluate the propfan structural integrity, source noise, cabin noise, flyover noise, and enroute noise. Thus, an extensive data base has been established for the development and validation of propfan aerodynamic and acoustic analyses.

In the PTA flight test program, the propfan propulsion system was mounted on the left wing of the modified GII aircraft. This location was chosen to avoid flowfield interference with the main propulsion Gulfstream engines and to permit systematic investigation of the propfan characteristics.[4] A nacelle tilt arrangement was employed to vary the inflow angle to the propfan. The variations in inflow conditions were used to evaluate the effects on cyclic stress of the propfan over a wide range of operating conditions. The inflow conditions also play an important role in the generation of noise. The three nacelle tilt angles of the test were − 3, − 1 (tilt down), and + 2 deg (tilt up). The average inflow angle is dependent on the airplane angle of attack, propfan upwash angle, and nacelle tilt. The complete nacelle tilt variation of 5 deg (− 3 to + 2 deg) provided an inflow angle variation of 5 deg.[5]

Acoustic and performance data were acquired over a wide range of operating conditions. The test points were specifically chosen to determine the near-field noise characteristics as a function of flight Mach number, altitude, propfan tip speed, power, and inflow angle.

The near-field acoustic data for the baseline design-point cruise ($M = 0.8$) case of − 1-deg nacelle tilt have been analyzed in detail.[5] The acoustic data measured on a wing boom outboard of the propfan show that the first five harmonics have maximum sound pressure levels (SPL) in the plane of the propfan. The SPLs decrease in level with increase in harmonic order and all have similar directional characteristics. The SPLs were also predicted using Hanson's frequency domain propeller noise radiation theory.[6] The predictions show that the SPLs are maximum at 0.25 diam aft of the propeller plane. The levels are overpredicted by about 3 dB.

The effects of nacelle tilt on the fuselage and wing boom SPLs were studied both at the cruise and takeoff conditions. Increasing nacelle tilt resulted in significant reductions in SPL at the fuselage for all tip speeds. At the wing boom, the SPLs were found to increase with increase in tilt angle. On the average, an acoustic sensitivity of about 1 dB/deg of nacelle tilt was observed. Predictions of the SPLs for the nacelle tilt test cases were also done by Hamilton Standard; however, the predicted fuselage and wing boom SPLs showed very little sensitivity to nacelle tilt angle.

Prediction of the effect of inflow angle on the SPLs requires accurate computation or measurement of the unsteady blade surface pressures. The linear analytical methods for computing the unsteady blade loading may not predict the loading

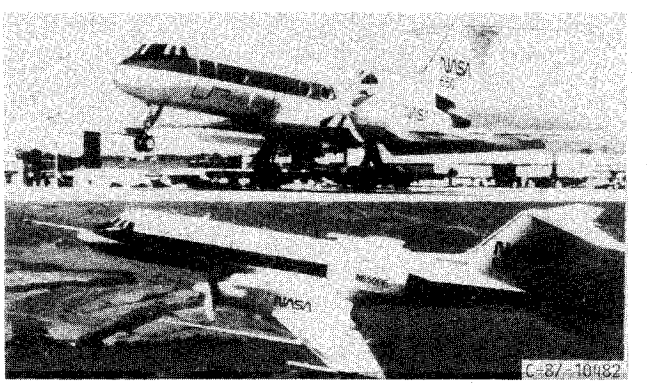

Fig. 1 SR7L propeller installed on the testbed aircraft.

Presented as Paper 89-1060 at the AIAA 12th Aeroacoustics Conference, San Antonio, TX, April 10–12, 1989; received May 15, 1989; revision received Nov. 8, 1989.

*Senior Supervisor, Aeromechanics Department.
†Chief, Propeller and Acoustics Technology Branch, Propulsion System Division.

accurately enough at higher inflow angles due to nonlinear processes involved. In the present paper, the unsteady blade pressures are computed by numerically solving the three-dimensional unsteady Euler equations. The only published three-dimensional unsteady Euler solution for the propeller at an angle of attack is that of Whitfield et al.[7] The emphasis in that work was on validation of the solution algorithm for different configurations. The present paper provides, for the first time, detailed unsteady Euler solutions of the propeller at an angle of attack. The angle-of-attack induced unsteadiness is illustrated in the form of chordwise, spanwise, and azimuthal pressure distributions.

Solution of the Unsteady Euler Equations

The unsteady three-dimensional Euler equations governing the inviscid flow through a propeller are solved using the solution procedure developed by Whitfield et al.[7,8] (The details may be found in the references cited. Here, only a brief mention of the technique will be made.) The equations in conservative differential form are transformed from a Cartesian reference frame to a time-dependent, body-fitted, curvilinear reference frame. The transformed equations are discretized employing a finite volume technique. An approximate Riemann solver is used for block interface flux definitions. A lower-upper (LU) implicit numerical scheme that possesses apparent unconditional stability is used to solve the discretized equations. The flowfield is represented by multiblock composite grids to overcome computer core memory limitations. The solution at each time step is updated by having only one block in memory while the other blocks are stored in solid-state storage devices (SSD).

Flow Configuration and Computational Grid

The configuration considered here is the eight blade 9-ft-diam SR7L propeller (Fig. 1) of the PTA program. The inflow angle chosen for the present computations is 4.6 deg (corresponding to nacelle tilt of + 2 deg in the PTA program). The direction of rotation of the propeller along with the axes of reference is shown in the figure.

Each blade passage is discretized employing a $71 \times 33 \times 11$ grid in the axial, radial, and circumferential directions, respectively. Each passage grid is divided into two blocks for computational convenience as mentioned before. Thus, 16 blocks of grids are employed to describe the entire propeller flowfield with 206,184 nodal points. Each blade surface has 35×21 (chordwise by spanwise) grid points with higher resolution near the leading and trailing edges. The solution presented here is for the cruise condition, Mach number = 0.801, and advance ratio 3.122, with an inflow angle of 4.6 deg.

Results and Discussion

The unsteady three-dimensional Euler equations have been solved (from an impulse start) for three complete revolutions of the propeller to get a reasonably accurate solution. The results of the third cycle are fairly stabilized as can be seen from Fig. 2. The figure shows the variation of the total power coefficient with azimuth angle. The total power coefficient becomes nearly constant during the entire third revolution of the propeller. The results of this cycle are analyzed further and presented. The predicted total power is about 8% higher than the measured value. No chordwise pressure measurements are available for a direct comparison of the predictions. However, the predictions of unsteady blade surface pressures employing the present solution technique were compared with data in Refs. 9 and 10 for two- and eight-bladed configurations, respectively, and the agreements were found to be fairly good. In Ref. 9, detailed comparisons of blade surface pressures (waveforms) for an angular inflow of 3 deg at two Mach numbers, 0.5 and 0.2, were made. At Mach 0.5, the predicted pressures on both the suction and pressure surfaces agreed well with data. At the low Mach number of 0.2, the sinusoidal response on the pressure side was well predicted, whereas the measured highly nonlinear response on the suction surface was not predicted. It was conjectured that such a highly nonlinear response could be the result of an unsteady, viscous flow separation phenomenon and would require a Navier-Stokes analysis. In Ref. 10, the predicted pressure waveforms at cruise conditions (Mach number = 0.8) for an inflow angle of 1.5 deg were compared with wind-tunnel measurements on a model propeller. A good agreement was obtained at most of the transducer locations.

Figure 3a shows the variation of the single-blade power coefficient with azimuth angle (ϕ) for two blades, one starting from $\phi = 0$ (or $\phi_s = 0$) position and other starting from $\phi = \pi$

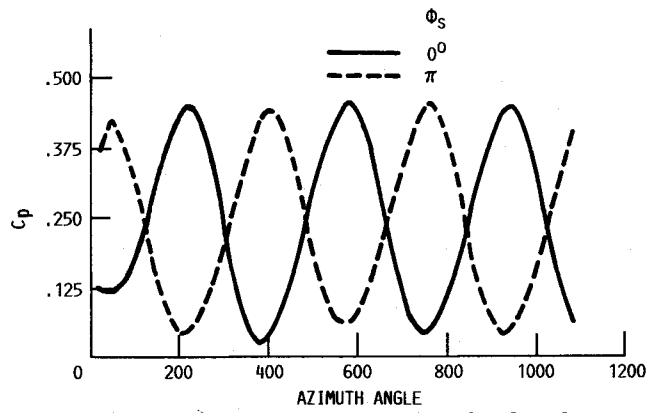

Fig. 3a Power per blade variation with azimuth angle.

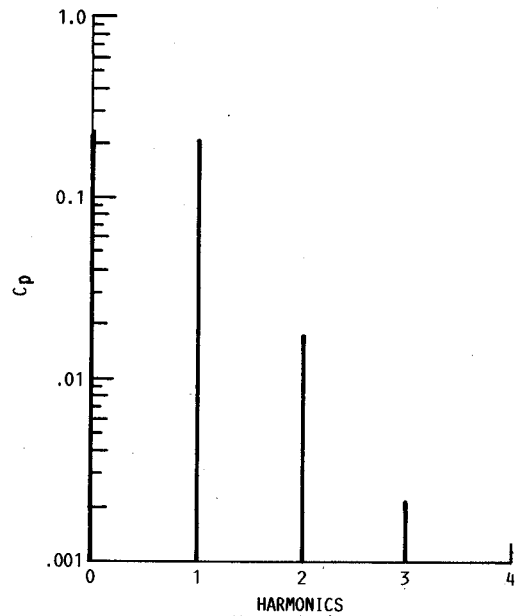

Fig. 3b Loading spectrum.

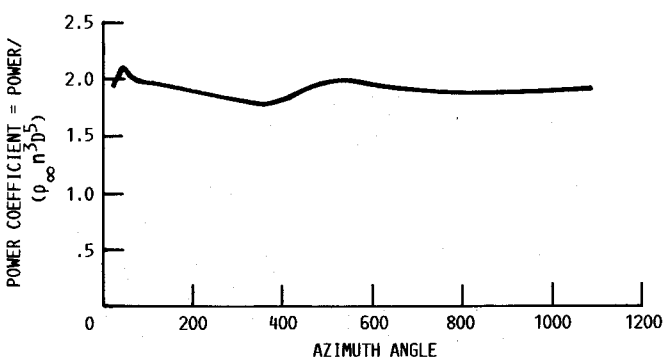

Fig. 2 Total power coefficient variation with azimuth angle.

(or $\phi_s = \pi$). The expected sinusoidal variation of the loading due to angle of attack ($\alpha = 4.6$ deg) is clearly exhibited. However, the variation of power during a cycle is significantly higher than one might expect. For the case of 4.6 deg inflow angle, the power coefficient per blade varies $\pm 81\%$ during a cycle. A careful look at the plot reveals additional details: the loading is not exactly sinusoidal, the loading is not minimum at $\phi = 0$, and the maximum is not at $\phi = \pi$, as originally believed. The rising portion of the curve lasts for about $9/8\ \pi$, whereas the falling portion of the wave lasts about $7/8\ \pi$. For the blade starting at $\phi = 0$, the minimum loading occurs at $\pi/8$ and the maximum loading occurs at about ($\pi/8 + 9/8\ \pi = 5/4\ \pi$) or 225 deg. These points have to be kept in mind during the analysis of the results.

A Fourier transform on the third-cycle loading gives the blade power coefficient CP as $CP = a_o - a_i \cos\omega t - b_i \sin\omega t$, where a_o, a_i and b_i are the Fourier coefficients. The loading spectrum shown in Fig. 3b indicates that the first harmonic dominates the loading. The oscillating part of the CP lags behind the motion of the blade by 14.4 deg.

For comparison purposes, a steady-state solution was obtained for the same advance ratio (3.122) and Mach number

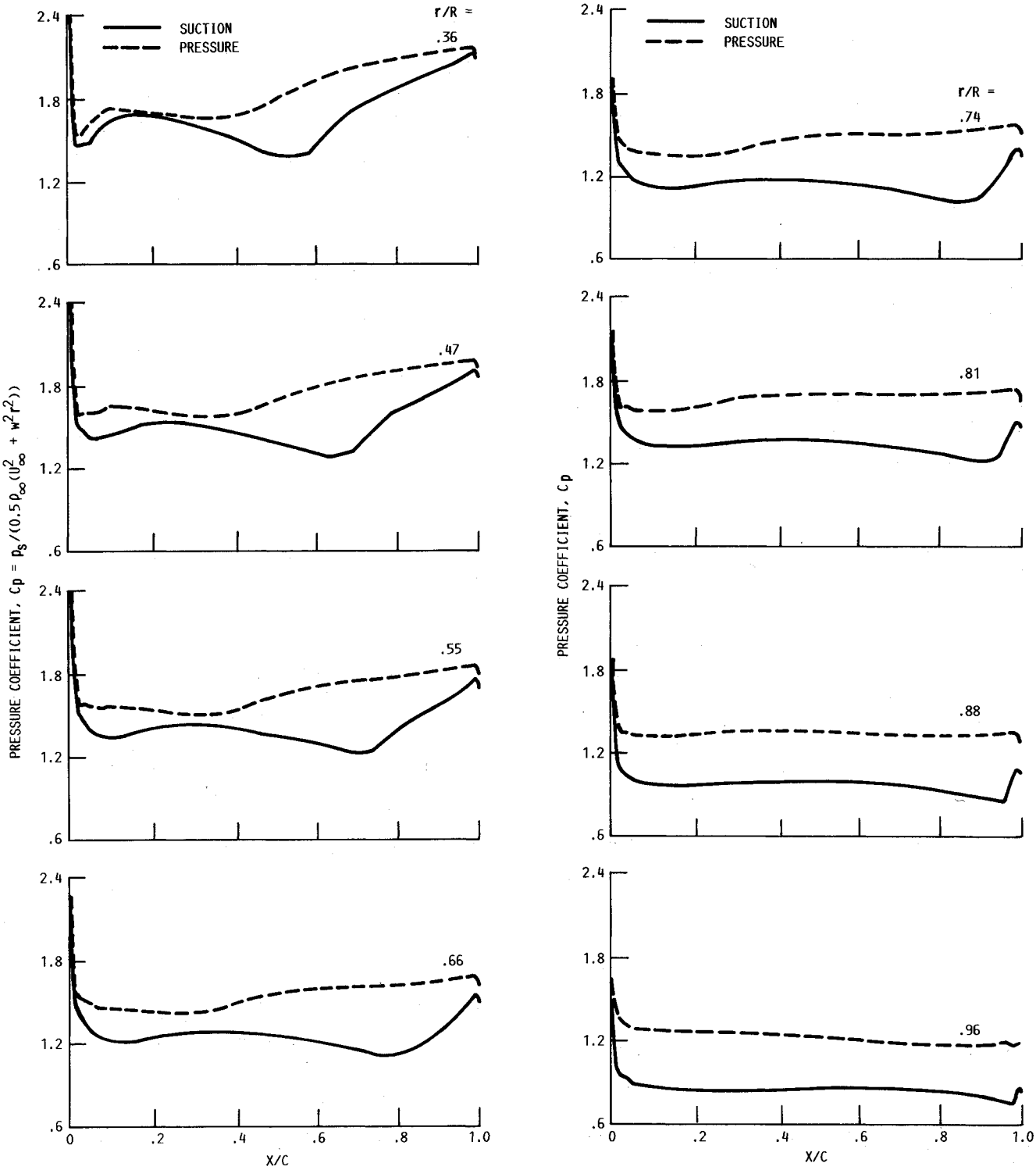

Fig. 4 Steady blade surface pressure distribution, $\alpha = 0$.

(0.801) but with zero angle of attack. The steady blade surface pressure distributions are shown in Fig. 4. The figure shows chordwise pressure distributions at eight spanwise locations. The unsteady blade surface pressure distributions presented in the succeeding figures will be at one or more of these spanwise locations. Thus, a direct comparison of the steady and unsteady pressure distributions can be made.

The detailed azimuthal variations of the chordwise loading and blade surface pressure distributions are illustrated in Figs. 5-10 for three radial stations namely, $r/R = 0.36$, 0.66, and 0.96. Figure 5 presents the chordwise loading variations as a function of azimuth angle at the radial station $r/R = 0.36$. At this radial station, the blade is negatively loaded for the front half (0-50%) of the chord length for about 3/8 of a revolution ($\phi = 0$, 45, 90 deg) and the loading is maximum at $\phi = 225$ deg. Thus, the chordwise loading undergoes a cyclic variation of substantial amplitude. The shape of the loading curve also changes enormously during the cycle. The reasons for this change become apparent from the actual blade surface pressures shown in Fig. 6 for the same radial and azimuthal locations. The trailing-edge shock appears on the suction sur-

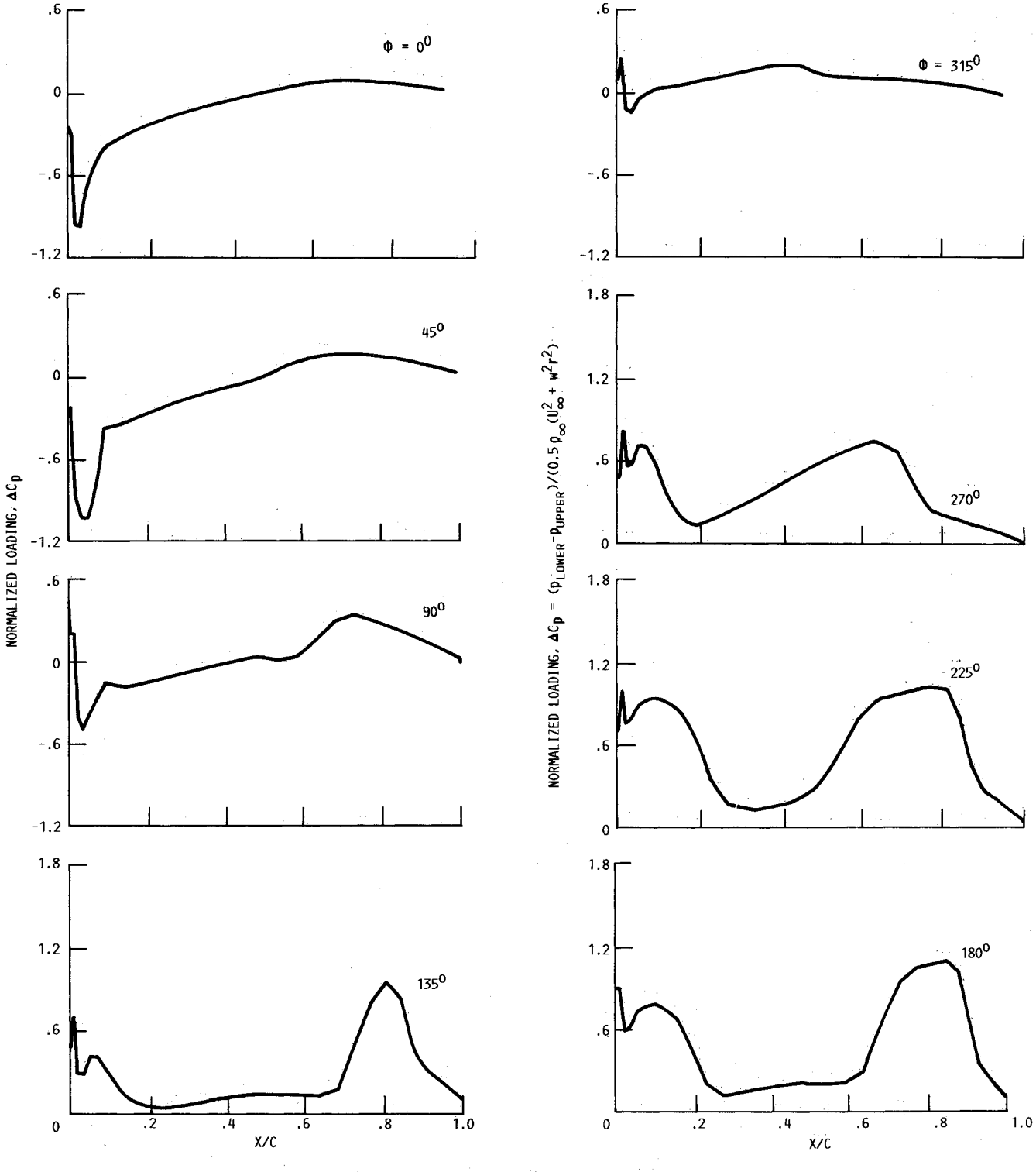

Fig. 5 Azimuthal variation of chordwise loading at $r/R = 0.36$.

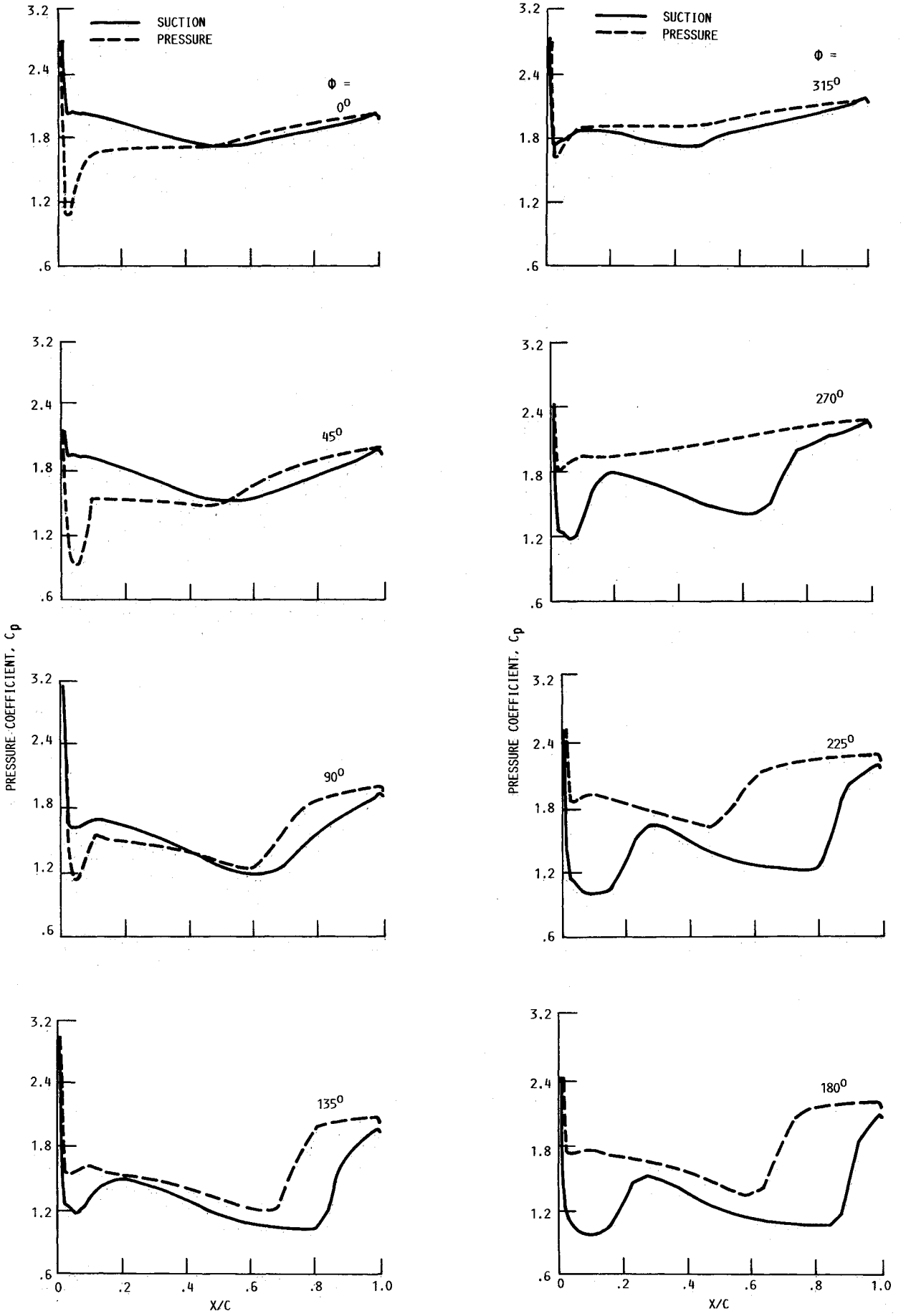

Fig. 6 Azimuthal variation of blade surface pressures at $r/R = 0.36$.

face for $\phi = 135$–270 deg, whereas the shock appears on (or extends to) the pressure surface for $\phi = 135$–225 deg. The dramatic changes in the loading pattern are clearly illustrated in this figure.

Figure 7 shows the azimuthal variation of chordwise loading distribution at $r/R = 0.66$. The part of the revolution during which significant negative loading exists is reduced for this radial station. A continuous change of the shape of the loading curve occurs throughout the revolution. The second half (50–100% chord) of the blade is highly loaded from $\phi =$ 90–225 deg. The blade surface pressures shown in Fig. 8 indicate the appearance of the trailing-edge shock for $\phi = 90$–270 deg and a pressure jump on the pressure side occurs only for $\phi = 90$–225 deg. Thus, for the two radial stations (0.36 and 0.66), the shocks appear only during parts of the cycle. It is also interesting to note that the shock on the pressure surface moves upstream as we go from $\phi = 90$–225 deg.

The periodic motion of shock waves on oscillating airfoils in transonic flow has been extensively studied and documented.[11] Three types of shock motion have been identified: 1) Sinusoidal shock wave motion (type A): The shock wave moves almost sinusoidally and exists during the complete cycle; 2) interrupted shock wave motion (type B): This motion is like

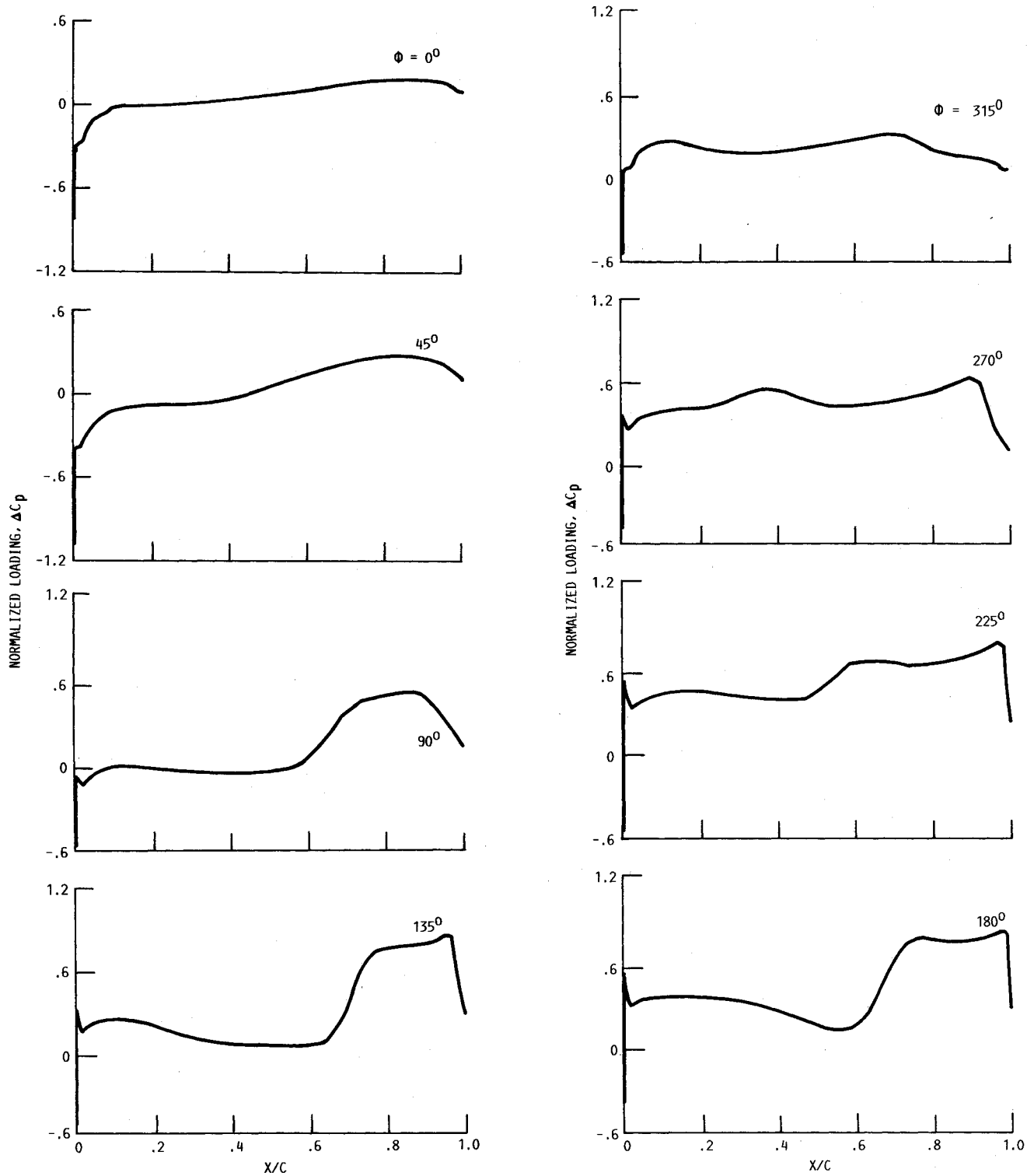

Fig. 7 Azimuthal variation of chordwise loading at $r/R = 0.66$.

type A but the shock disappears during part of a cycle; and 3) upstream propagated shock wave motion (type C): At slightly super critical Mach numbers, periodically a shock wave is formed on the upper surface of the airfoil and moves upstream while increasing in strength. No such detailed experimental study exists for the three-dimensional transonic flows of the type considered in this paper. But the results presented in Figs. 6 and 8 suggest that shock motions similar to type B and type C occur in the unsteady three-dimensional transonic flows.

The azimuthal variation of chordwise loading at the radial station $r/R = 0.96$ is shown in Fig. 9. At this radial station, the changes in the shape of the loading curve are marginal, compared to those at $r/R = 0.36$ and 0.66. However, the location of the maximum loading moves from a point close to the trailing edge to a point near the leading edge as we go from $\phi = 45$–315 deg. The blade surface pressure variations shown in Fig. 10 indicate that the shocks have diffused before reaching this radial station. It is interesting to note that the tip region is significantly loaded through the complete revolution of the blade.

Figures 11–14 show the radial variation of the chordwise pressure distribution for four azimuthal angles, $\phi = 0$, 90, 180, and 270 deg, respectively. The radial variations of the

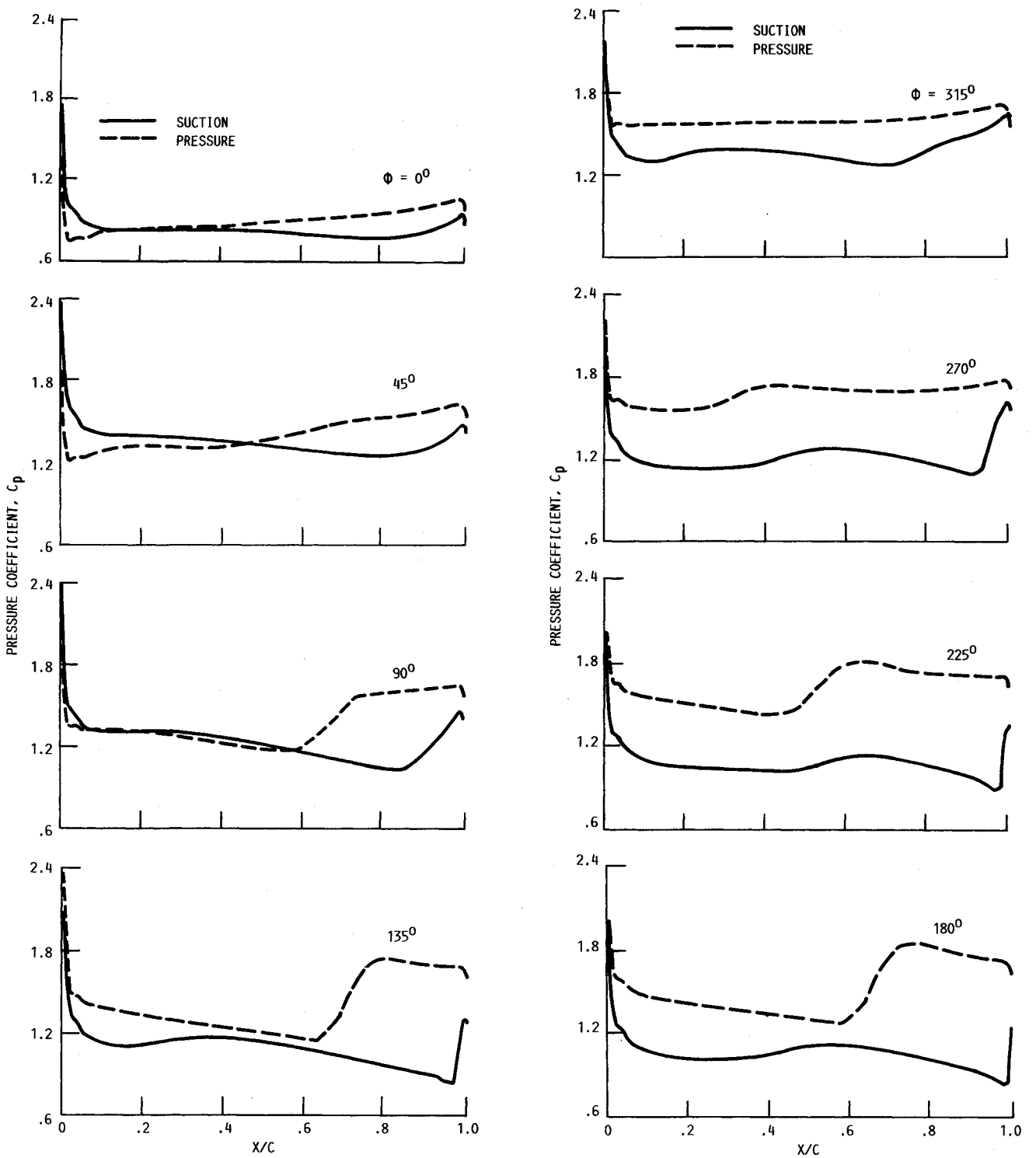

Fig. 8 Azimuthal variation of blade surface pressures at $r/R = 0.66$.

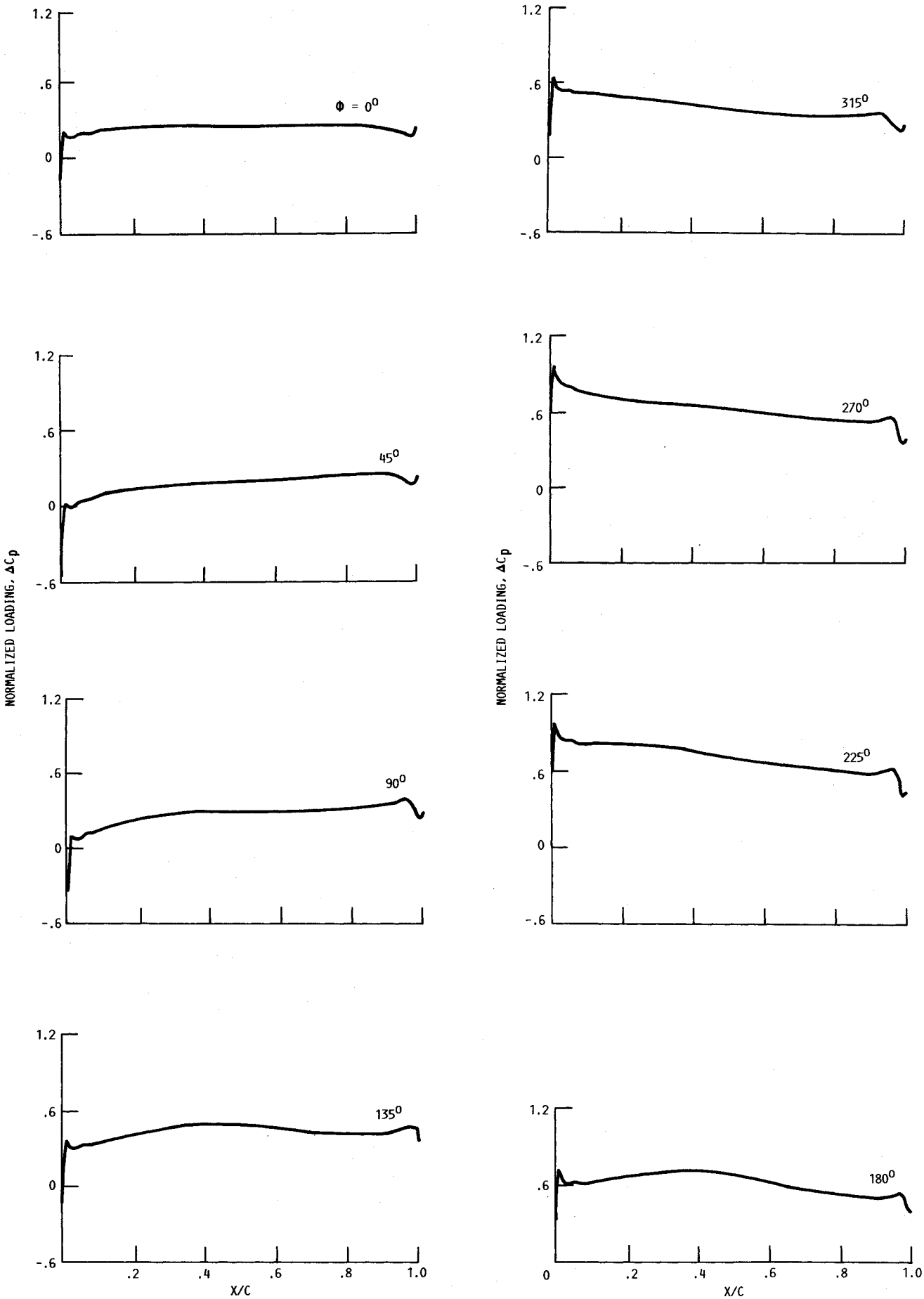

Fig. 9 Azimuthal variation of chordwise loading at $r/R = 0.96$.

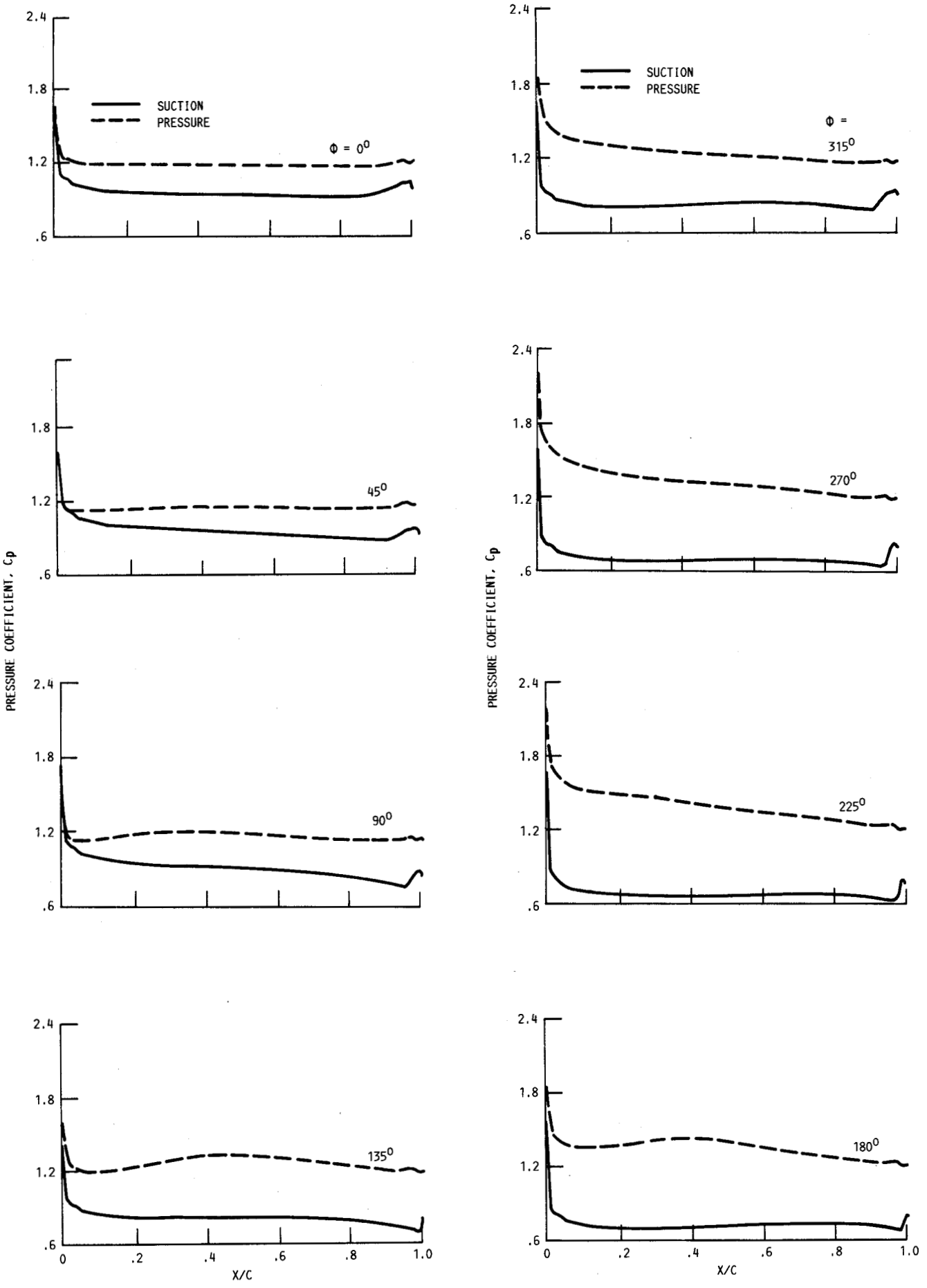

Fig. 10 Azimuthal variation of blade surface pressures at $r/R = 0.96$.

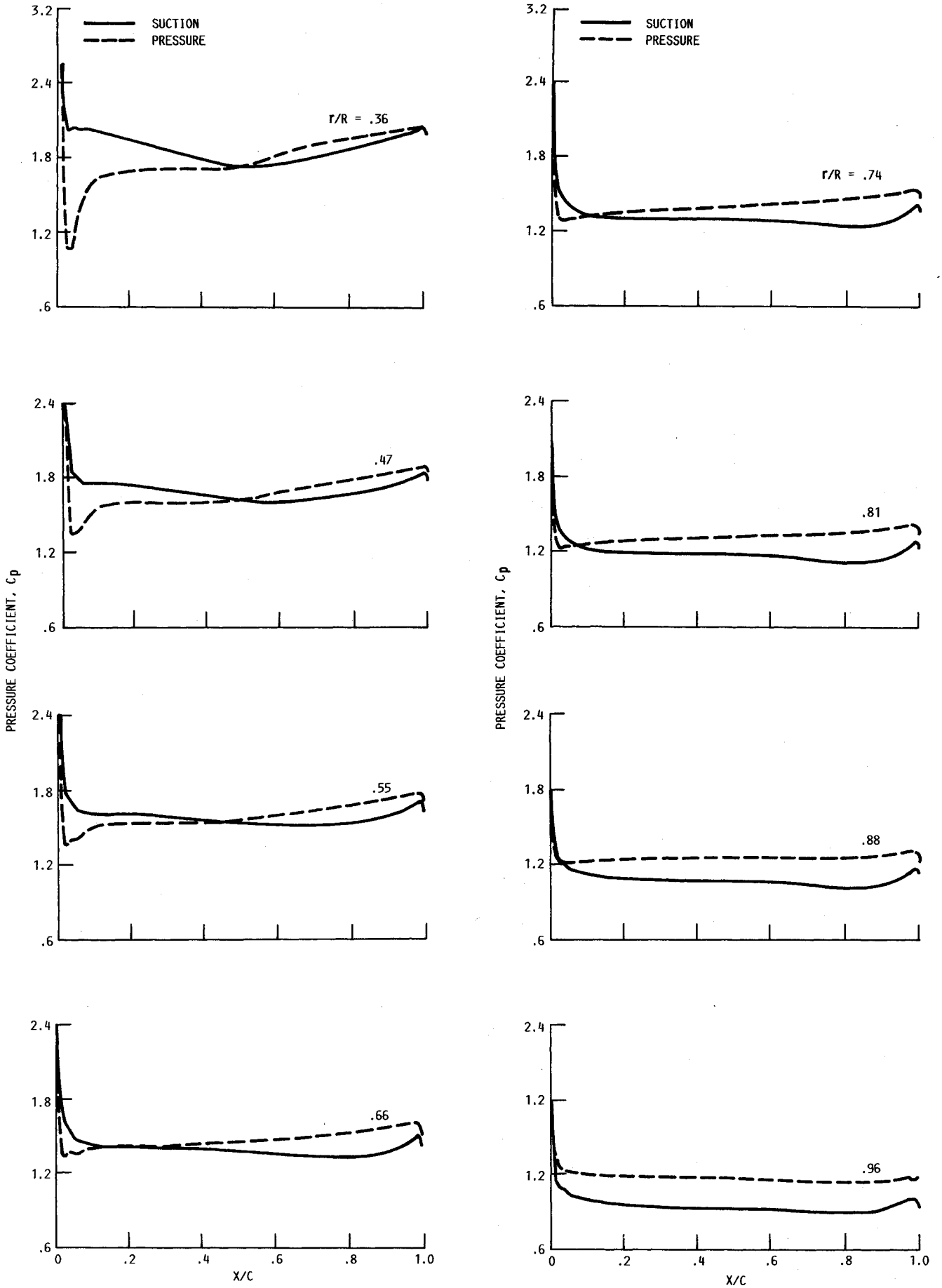

Fig. 11 Spanwise variation of blade surface pressures at $\phi = 0$ deg.

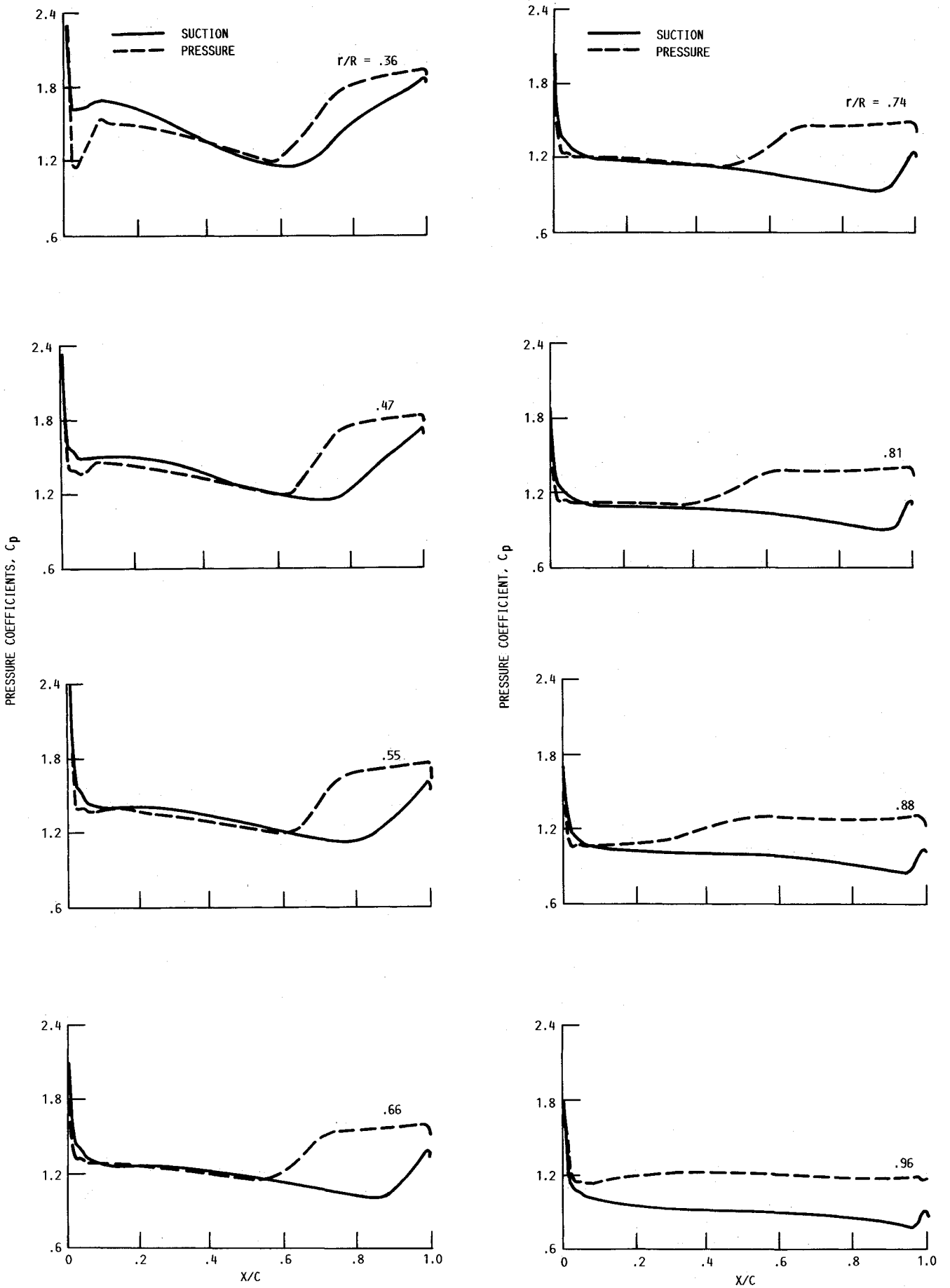

Fig. 12 Spanwise variation of blade surface pressures at $\phi = 90$ deg.

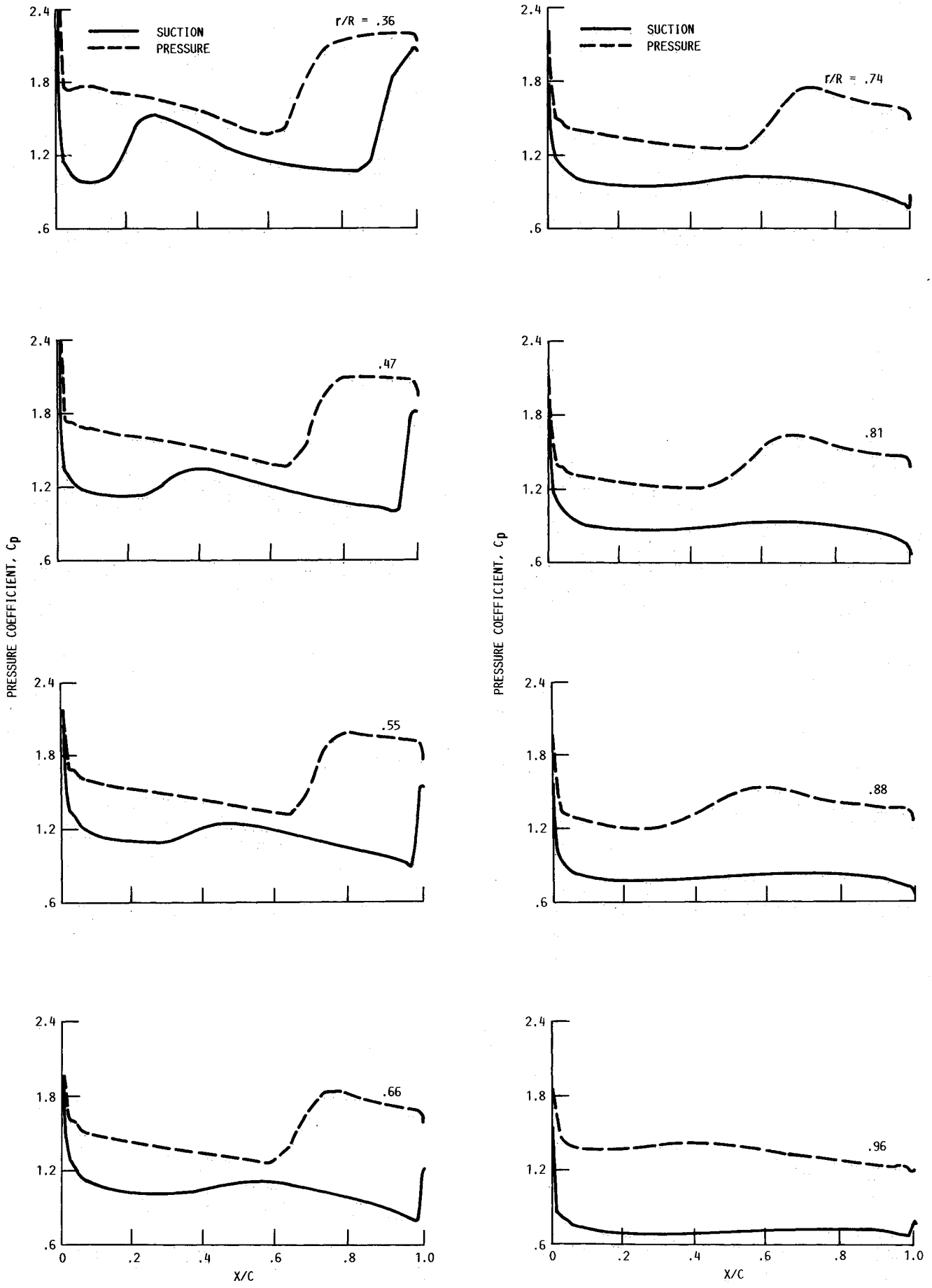

Fig. 13 Spanwise variation of blade surface pressures at ϕ = 180 deg.

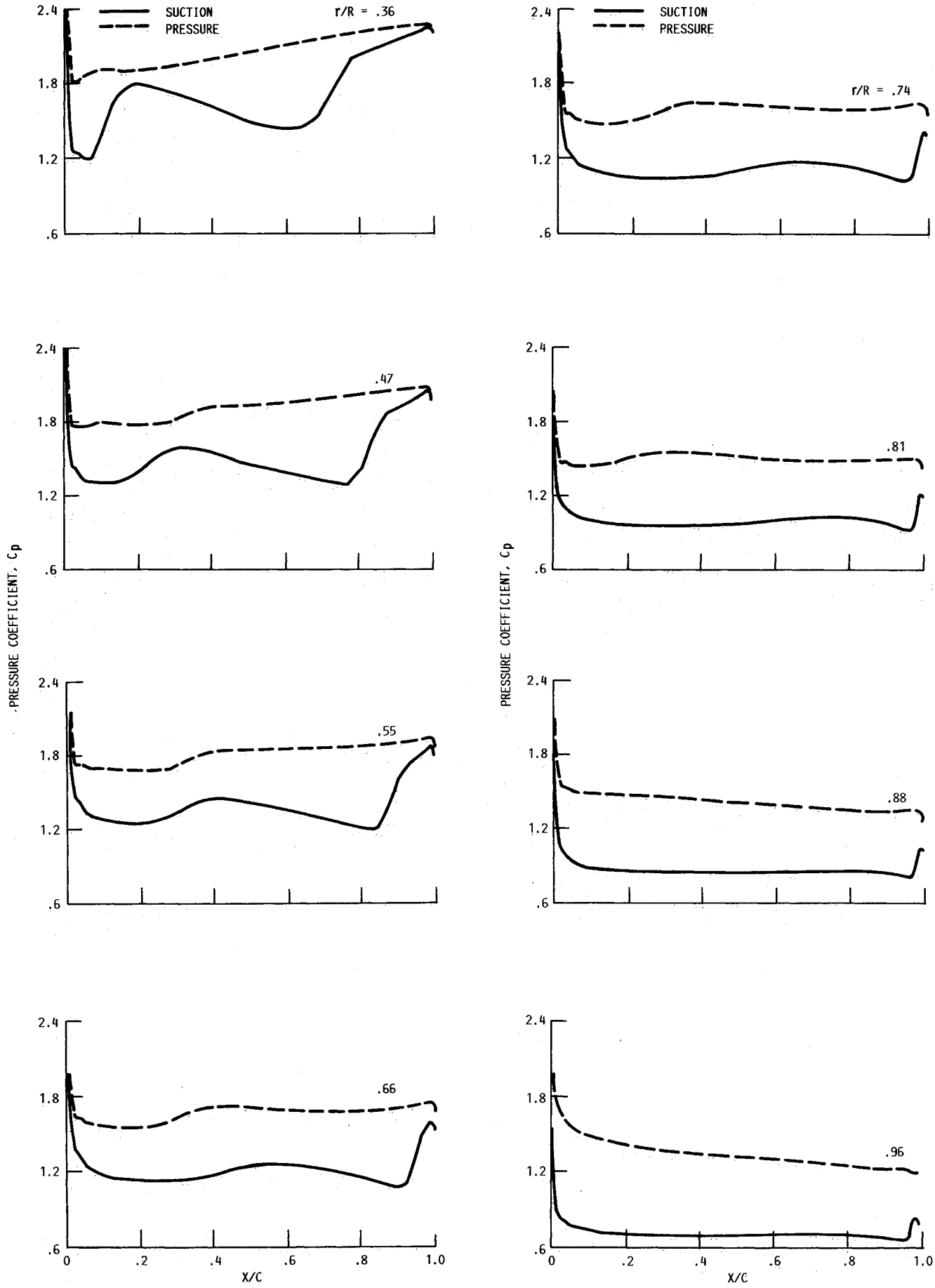

Fig. 14 Spanwise variation of blade surface pressures at $\phi = 270$ deg.

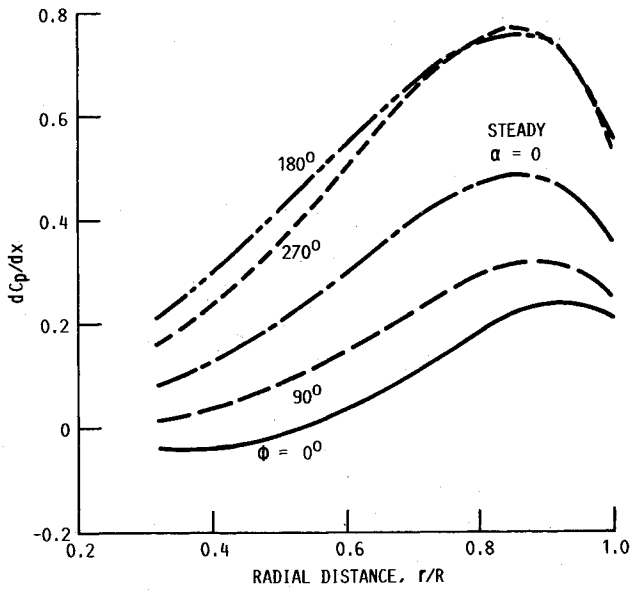

Fig. 15 Elemental power coefficient.

chordwise loading distribution at $\phi = 0$ deg are shown in Fig. 11. At this azimuthal location, the blade is very lightly loaded throughout the span. A small negative loading exists almost up to $r/R = 0.80$, which is due to the low local flow incidence angle produced by the angle of attack of the propeller. Figure 12 shows the radial variations of the chordwise pressure distributions at $\phi = 90$ deg. Here, shocks exist both on the suction and pressure surfaces from the hub region to almost 90% span. Up to 80% span, the loading is primarily on the rearward half (50–100% chord) of the blade.

The spanwise variation of the loading at $\phi = 180$ deg is shown in Fig. 13. At this location, the blade loading experiences a near maximum. Also at this azimuthal location, shocks appear on both suction and pressure surfaces from the hub region. However, on the suction surface, the trailing-edge shock is diffused beyond about 62% span. The shock on the pressure surface persists to 80% span, as for the $\phi = 90$ deg position. Figure 14 shows the spanwise variations of the loading for $\phi = 270$ deg. Here, no shock exists on the pressure side of the blade. On the suction surface, a shock appears at about 70% chord at the radial station near the hub, $r/R = 0.36$. With increasing spanwise distance, the shock moves toward the trailing edge. The four figures (Figs. 11–14) demonstrate that the blade loading changes significantly in the chordwise, radial, and azimuthal directions during a revolution due to the angular inflow to the propeller.

The variations of the elemental power coefficient (dCp/dx) for the four azimuthal locations ($\phi = 0$, 90, 180, and 270 deg) are shown in Fig. 15. The general shape of the curve is the same as that obtained for a steady flow. The magnitude of dCp/dx at any radial distance ($x = r/R$) depends on the azimuthal location. Also shown in the figure is the curve for the steady flow ($a = 0$) solution. It is seen that the magnitude of the cyclic variations of loading depends on the spanwise location.

The azimuthal variations of blade pressure coefficient at specified points along the chord at the radial station $r/R = 0.66$ are shown in Fig. 16. It can be seen that the response at the individual points $X/C = 0.036$, 0.125, 0.53, 0.63, and 0.84 is not exactly sinusoidal. The extent of the deviation from the sinusoid depends on the chordwise location and the surface (suction or pressure surface) on which the point is located. The departure from the sinusoidal behavior may be due to the high inflow angle and the presence of shock waves. It should also be noted that the instantaneous pressure coefficients are plotted in this figure rather than the fluctuations about the mean value of the pressure.

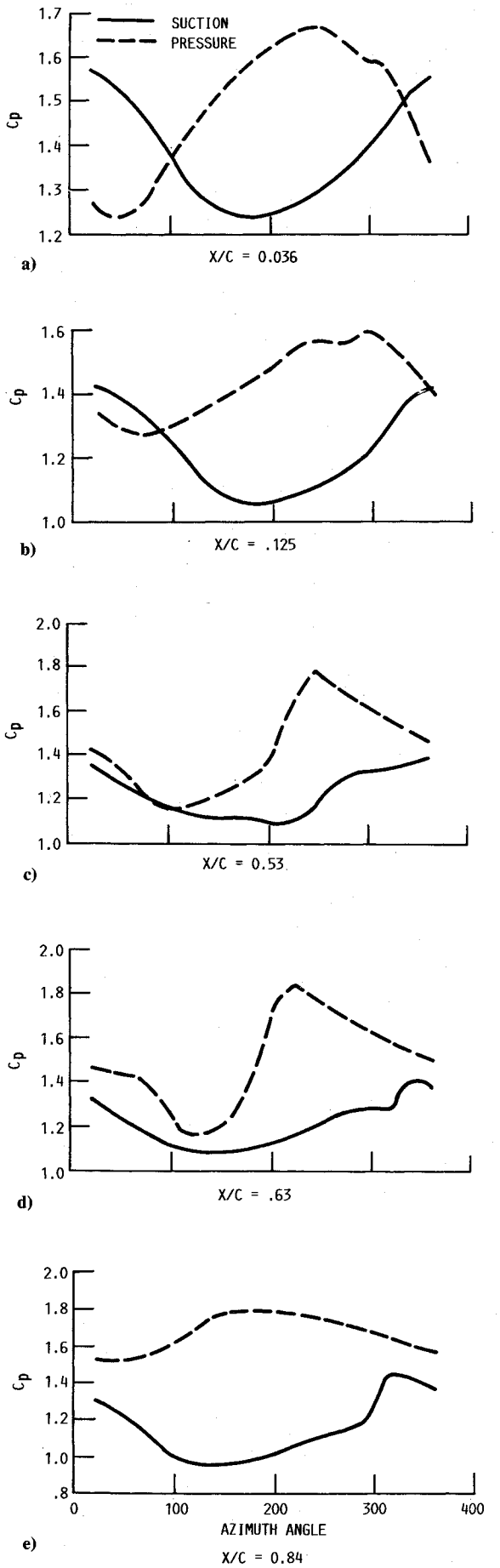

Fig. 16 Blade response at different axial locations on $r/R = 0.66$.

Concluding Remarks

A numerical solution of the unsteady three-dimensional Euler equations has been obtained for the flow through a propeller at an angle of attack to the mean flow. The results show the highly nonlinear nature of the loading variations during a revolution. For parts of the revolution, the blade is very lightly loaded, whereas, for other parts, it is highly loaded with shocks appearing on both surfaces of the blade. The sound pressure levels, directivity, and azimuthal variation will be studied next employing the unsteady blade pressure distribution obtained here.

Acknowledgments

The work of the first author was supported under contract NAS3-25266 with the NASA Lewis Research Center. The authors wish to acknowledge the many helpful discussions with D. Hoyniak, M. Janus, D. Huff, and B. Clark during this research.

References

[1]Bushnell, P., "Measurement of the Steady Surface Pressure Distribution of a Single Rotation Large Scale Advanced Propfan Blade at Mach Numbers from 0.03 to 0.78," NASA CR-182124, July 1988.

[2]Bushnell, P., Gnuber, M., and Parzych, D., "Measurement of Unsteady Blade Surface Pressures on a Single Rotation Large Scale Advanced Propfan with Angular and Wake Inflow at Mach Numbers from 0.02 to 0.70," NASA CR-182123, Oct. 1988.

[3]Cambell, W. A., Wainauski, H. S., and Bushnell, P. R., "A Report on High Speed Wind Tunnel Tests of the Large Scale Advanced Propfan," AIAA Paper 88-2802, July 1988.

[4]Poland, D. T., Bartel, H. W., and Brown, P. C., "PTA Flight Test Overview," AIAA Paper 88-2803, July 1988.

[5]Lockheed Aeronautical Systems Company, "Propfan Test Assessment: Flight Test Results Review," NASA Lewis Research Center, Nov. 1988.

[6]Hanson, D B., "Near-Field Frequency Domain Theory for Propeller Noise," *AIAA Journal*, Vol. 23, No. 4, 1985, pp. 499–504.

[7]Whitfield, D. L., Swafford, T. W., Janus, J. M., Mulac, R. A., and Belk, D. M., "Three Dimensional Unsteady Euler Solutions for Propfans and Counter Rotating Propfans," AIAA Paper 87-1197, June 1987.

[8]Janus, J. M., and Whitfield, D. L., "A Simple Time Accurate Turbomachinery Algorithm with Numerical Solutions of Uneven Blade Count Configuration," AIAA Paper 88-0206, Jan. 1988.

[9]Nallasamy, M., and Groneweg, J. F., "Unsteady Blade Surface Pressures on a Large-Scale Advanced Propeller: Prediction and Data," AIAA Paper 90-2402, 1990.

[10]Heidelberg, L. J., and Nallasamy, M., "Unsteady Blade Pressure Measurements for the SR-7A Propeller at Cruise Conditions," AIAA Paper 90-4022, 1990.

[11]Tijdeman, H., and Seebass, R., "Transonic Flow Past Oscillating Airfoils," *Annual Review of Fluid Mechanics*, Vol. 12, 1980, pp. 181–222.